arXiv:1703.07128v2 [cond-mat.mtrl-sci] 12 Apr 2017

Effects of atoms and molecules adsorption on electronic and magnetic properties of s-triazine with embedded Fe atom: DFT investigations

Yusuf Zuntu Abdullahi[a,b,*], Tiem Leong Yoon[a], Mohd Mahadi Halim[a], Md. Roslan Hashim[a], Thong Leng Lim[c]

[a]*School of Physics, Universiti Sains Malaysia, 11800 Penang, Malaysia*
[b]*Department of Physics, Faculty of Science, Kaduna State University, P.M.B. 2339 Kaduna State, Nigeria*
[c]*Faculty of Engineering and Technology, Multimedia University, Jalan Ayer Keroh Lama, 75450 Melaka, Malaysia*

Abstract

We employ first-principles calculations to study the mechanical, geometrical, electronic and magnetic properties of Fe atom embedded s-triazine ($Fe@C_6N_6$) system under the influence of external environment. Our results show that the binding energy of $Fe@C_6N_6$ can be modulated by an applied tensile deformation and perpendicular electric field. The non-magnetic semiconducting property of pure s-triazine sheet (C_6N_6) is found to change upon embedding of Fe atom in the porous site of the sheet. It is revealed that the $Fe@C_6N_6$ system exhibits half-metallic electronic character with a magnetic moment in the the order similar to that of an isolated Fe atom. Furthermore, electronic and magnetic properties of the $Fe@C_6N_6$ systems are preserved up to a maximum value of 10 V/nm in electric field strength and 6% tensile strain. Interestingly, we find that the half-metallic electronic character of $Fe@C_6N_6$ system can be tuned into a semiconductor via adsorption of atoms and molecules into the $Fe@C_6N_6$ system. The magnetic moment of $Fe@C_6N_6$ with adsorbed atoms/molecules is also modified. Our findings may serve as a guide for future applications of $Fe@C_6N_6$ structures in spintronics devices.

Keywords:

*Corresponding author
Email addresses: yusufzuntu@gmail.com (Yusuf Zuntu Abdullahi), tlyoon@usm.my (Tiem Leong Yoon)

1. Introduction

Currently there is an intense search for suitable substrates for transition metal (TM) atoms encapsulation [1],[2],[3]. The central concern in the encapsulation is to ensure that the substrate remains inert and strongly binds to the TM atoms. Moreover, the appropriate substrate is expected to preserve its intrinsic properties and that of bound TM atoms. Two-dimensional (2D) carbon-based and related surfaces with compacted hexagonal rings have been a frequent choice for trapping TM atoms [4],[5],[6],[7] due to their desirable surface properties. Numerous works have so far been done to investigate the stable geometries and electronic properties of TM atoms adsorption on graphene and boron nitride sheets [7],[8],[9]. However, their reports have shown that the adatoms tight weekly on these 2D surfaces as a result of low adsorption energies. Additionally, the large surface free energy of the TM atoms would make them aggregate easily to form cluster on these surfaces. To ensure the immobility of the TM atoms on the surface, various defect sites have been proposed [8]. Creation of defect sites would presumably bind the TM atoms firmly to the surface. However, forming regular defect sites experimentally may not be possible due to influence of external environment. Thus, much efforts have been made to synthesis 2D materials with inherently defined porous sites [10].

Among the recently synthesized porous 2D materials [11], graphitic carbon nitride (CN) sheet has received much attention [12], [13]. This is due to its potential as a right candidate for various applications [14],[15],[16],[17],[18]. Graphitic CN belongs to a group of allotrope with a common chemical formula g-C_xN_y, where x and y represent the number of C and N atoms in the unit cell. For example, single triazine-based graphitic CN has a chemical formula g-s-C_3N_4 whereas tri-single triazine-based (heptazine) graphitic CN is named g-t-s-C_3N_4 [13]. The hexagonal rings in the unit cell of heptazine are compacted in an abreast manner. s-triazine with a chemical formula g-C_6N_6 is another allotrope of graphitic CN in which two of its hexagonal rings (g-C_3N_3) are separated via a C-C bond [12]. Depending on the composition of C and N in the hexagonal rings and unit cell, these allotropes can have different electronic properties ranging from semiconducting to half-metallic. For instance, triazine-based g-C_4N_3 is another allotrope of graphitic CN which possess a ferromagnetic ground state with half metallic electronic character

[19] whereas the rest of the allotropes are non-magnetic with wide or small band gaps [12],[13].

To search for a suitable spintronic material such as diluted magnetic semiconductor, first-principles calculations of TM atoms embedded in semiconducting CN sheet have been performed [1],[2],[3]. Choudhuri *et al.*. recently reported the findings of TM embedded g-C_3N_3 (TM@g-C_3N_3) systems based on density functional theory (DFT) [20]. The TM atoms (Cr, Mn and Fe) embedded g-C_3N_3 systems are found to be dynamical, thermally and mechanically stable. Their report also show that Cr, Mn and Fe embedded in the g-t-C_3N_3 systems exhibit high temperature ferromagnetism and high magnetic anisotropy energy (MAE) with a peak value per atom occurring in Cr@g-t-C_3N_3.

TM embedded graphitic carbon nanostructures can also be used for heterogeneous catalysis, hydrogenation of CO_2 and as membrane for separation of gases [21],[22],[23],[24],[25]. A recent theoretical study predicts excellent catalytic activities for single atomic catalyst (SAC) of TM embedded C_2N systems [24]. Additionally, an effective catalysis of hydrogenation of CO_2 into methanol on the copper embedded graphene system has been demonstrated by Sirijaraensre and Limtrakul [25]. Although good catalytic behavior has been reported for the SAC of TM embedded C_2N systems, a comprehensive understanding of various types of atoms and molecules adsorbed onto their surfaces is still lacking. In this work, we investigate the structural, electronic and magnetic properties of Fe embedded s-triazine sheet with various adsorbed atoms and molecules. We begin by analyzing the Fe embedded s-triazine without the adsorbed atoms and molecules. Then, we introduce these atoms (C,N,O,H) and molecules ($CH_4, N_2, O_2, H_2, CO, CO_2$) at a distant height above the porous site at which the Fe is situated. The relaxed Fe embedded s-triazine with adsorbed atoms and molecules systems are then further analysed.

2. Conputational method

We use QUANTUM ESPRESSO package [26] to carry out spin-polarised DFT [27] calculations within Perdew-Burke-Enzerhof (PBE) approximation [28]. Ultrasoft pseudopotential method is employed to treat the core and valence electrons of C, N, and Fe (semi-core included) atoms [29]. A plain wave basis set with kinetic energy cut-off of 550 eV was used to expand the wave functions. Marzari-Vanderbilt smearing method with Gaussian spreading

is employed [30] to aid the convergences of our systems. The Brillouin zone (BZ) is sampled with $8\times8\times1$ and $15\times15\times1$ Mankhorst-Pack k-point meshes for the self-consistent field and density of state calculations respectively [31]. The planar sheet is treated with periodic boundary condition and a thick vacuum space of 16 Å along the z-direction to avoid interaction between periodic layers. All geometries are fully relaxed using the BFGS quasi-Newton algorithm until Hellmann-Feynman force tolerance on each atom was smaller than 0.05 eV/Å.

The optimized geometries of 2×2 pure s-triazine sheet (C_6N_6) and Fe embedded C_6N_6 sheet (Fe@C_6N_6) are displayed in Fig. 1(a). All N atoms have sp^3-like hybridized structure, whereas each C atom which is bonded to three atoms has sp^2-like hybridized structure. The relaxed C-C bond length d linking the s-triazine units in Fe@C_6N_6 system and C-N bond lengths l in the embedded Fe atom cavity are in the range of 1.47-1.50 Å and 1.35-1.37 Å respectively. The calculated values agree well with the reported results [12]. The optimized lattice constant in the Fe@C_6N_6 is found to be 14.20 Å.

3. Results and Discussions

We used the expressions in Eq. (1) to compute the mechanical properties, such as in-plane stiffness Y (Young modulus), and Poisson's ratio v:

$$\begin{aligned} Y &= m_{11}\left(1-v^2\right) \\ v &= \frac{m_{12}}{m_{11}}. \end{aligned} \tag{1}$$

The variables m_{11}, m_{12}, (known as elastic constants) can be deduced from Eq. (2).

$$\begin{aligned} m_{11} &= \frac{1}{A_0}\left(\frac{\partial^2 E}{\partial s^2}\right)\Big|_{s=0} \quad (\text{uni}-\text{axial}) \\ 2\left(m_{11}+m_{12}\right) &= \frac{1}{A_0}\left(\frac{\partial^2 E}{\partial s^2}\right)\Big|_{s=0} \quad (\text{bi}-\text{axial}) \end{aligned} \tag{2}$$

where A_0, E, and s are equilibrium unit-cell area, strain energy and applied deformation. At each 0.005 applied deformation (within the harmonic region for both bi- and uni-axial tensile strains, see Fig. 2) in the xy-plane, the structure is fully relaxed. The calculated in-plane stiffness is 1193.2 GPa·Å (= 119.32 N/m), lower than the in-plane stiffness of pure heptazine sheets

[13]. The Poisson's ratio 0.18 is in the same order as that of graphene sheet [32]. The bulk modulus is determined from the product of equilibrium area and the second gradient of deformation energy with respect to area of the $Fe@C_6N_6$ system, which is written as

$$G = A \times \left(\frac{\partial^2 E}{\partial A^2} \right) \Big|_{A_m} \tag{3}$$

The variables in the Eq. (3) are defined as follows: A, U and A_m represent the area of the $Fe@C_6N_6$ sheet, the bi-axial deformation energy and the equilibrium area of $Fe@C_6N_6$ respectively. The calculated bulk modulus 86.49 N/m is less than the value for Mn-CN1 system reported in [1]. The difference in the calculated elastic constants in comparisons with previously related structures can be related to the weakening in the bonding networks of the hexagonal rings in the structures. In Table 2 we show the values of binding energy E_b and the structural parameters h and d obtained for different deformations in the range $\pm$ 2%. By applying strain, the height h (difference between the height of Fe and the average height of all atoms in the C_6N_6 sheet) value of the Fe in the relaxed $Fe@C_6N_6$ sheet do not change. Hence, approximately zero h confirms the planar structure of the $Fe@C_6N_6$ sheet. E_b is determined from Eq. (4) which is given by:

$$E_b = (E_{C_6N_6} + E_{Fe}) - E_t \tag{4}$$

where E_t, $E_{C_6N_6}$ and E_{Fe} denote the total energy of $Fe@C_6N_6$ system, the energy of bare C_6N_6 sheet, and the total energy of an isolated Fe atom. E_b for unstrained $Fe@C_6N_6$ system is equal to 4.73 eV. Our computed E_b value is consistent with the previous work [33]. It can also be seen that the $Fe@C_6N_6$ structure is more stable for positive binding energy and attained metastable state at a maximum 6% tensile strain. It is clearly shown in Table 2 that binding energy at a metastable state which is 6% tensile strain is found to be negative. The decrease in binding energy as a function of tensile strain can be explained as follows. Based on the definition of strain energy E (i.e., product of square of strain and the elastic constants) under harmonic deformations, an increasing E value stands for energetically favorable elastic moduli. Thus, for an increasing negative strain energy E of the $Fe@C_6N_6$ system (see Table 2), the binding energy according to Eq. (4) should correspondingly decrease. Table 2 illustrates the uniform increase in d_{Fe-N} and d bond lengths as a result of distortion in the $Fe@C_6N_6$ structure caused by the tensile deformations.

It is known that pure C_6N_6 sheet is a non-magnetic semiconductor, thus the induced magnetism in the Fe@C_6N_6 system is mainly from Fe atom (see M_{Fe} in Table 2). For unstrained Fe@C_6N_6 system, the estimated magnetic moment per unit cell is 3.74 μ_{B}, which is consistent with the recent report [33]. The magnetic moments are also evaluated for different applied tensile strains. It can be seen in Table 2 that the magnetic moment is less sensitive to the applied strain. This shows that the interaction between the Fe atom and the surrounding atoms in the porous site did not reduce the number of unpaired electrons in the d orbital of Fe atom. According to the results from Lowdin's charge analysis [34], the charge transfer Q into C_6N_6 sheet is contributed mainly by s, p orbitals of Fe atom. There is also a mixed bonding nature (ionic and covalent bonding) which is depicted in the charge-density difference plot (see Fig. 1(c)) by charge depletion between the atoms and localisation around the most elecronegative N atoms.

To analyze the modulation on the electronic properties of the Fe-embedded s-triazine system, we plotted the electronic band structure and corresponding total and projected density of states. As can be clearly seen in Fig. 3(i), pure C_6N_6 is nonmagnetic semiconductor. If Fe atom is embedded in the porous site of the C_6N_6 sheet, the electronic and magnetic properties are modulated. Fig. 4(a)-(f) show spin-polarised band structure, total density of states (TDOS) and corresponding projected density of state (PDOS) of Fe@C_6N_6 unstrained system. The figures portray half metallic electronic character of the Fe@C_6N_6 system. We can infer that the half-metallic character in Fe@C_6N_6 system is a result of electron transfer from Fe sub-orbital induced by ionic interaction between the Fe and the C_6N_6 sheet. The minority band structure in Fig. 4(a) confirms the half-metallic character which shows flat energy spectrum crossing over the Fermi level at conduction band minimum. From the PDOS plots, we can observe a dominant features of Fe atom s-, d- sub-orbitals as well as small contributions by p_z- of the surrounding six N atom in the Fermi level. At approximately -1.5 eV the bonding orbitals are contributed mainly by sp-like orbitals of the six N atoms, and the $d_{xy}, d_{x^2-y^2}$ orbitals of Fe atom in the majority spin state. Around -3.5 eV there is a mixed hybridization which is dominated by d-orbitals of the Fe atom in the majority spin state and s-, p_z-like orbitals of the surrounding N atoms in both majority and minority spin state.

When subjected to variations in external environment, i.e. symmetric tensile deformation (up to 6% bi-axial tensile strain, see Table 2) and application of electric field (up to a maximum of 10 V/nm, see Fig 3(iii)),

the half-metallic electronic character and magnetic moment of Fe@C_6N_6 system are preserved. On the other hand, binding of Fe atom in Fe@C_6N_6 is enhanced as larger electric field strength is applied. The resulting higher energy of Fe@C_6N_6 system which corresponds to an increase E_b can be related to repulsive effect between the p_x, p_y orbitals of N atom and the d_{xy}, $d_{x^2-y^2}$ orbitals of Fe atom. This repulsion moves p_z orbital towards higher energy and hence the system energy increases.

4. Adsorption of atoms and molecules on Fe embedded striazine sheet

The optimized stable geometries of Fe-embedded s-triazine with adsorbed atoms (C,N,O,H) and molecules ($CH_4, N_2, O_2, H_2, CO, CO_2$) systems are displayed in Fig. 5 and 6. All atoms in the system are allowed to move freely without any constraint during the structural relaxation. We also listed the geometric parameters of the stable systems in Table 3. For the adsorbed atoms, the parameter h_{Fe-X} (where X represents atoms/molecules) are within chemisorption bonding height. These calculated bond lengths are indications of interaction between the embedded Fe atom and the adsorbed atoms. Nitrogen atom being the most electronegative has the shortest adsorption height, hence the magnetic moment per unit cell is also the lowest due to the strong interaction. The estimated heights of h_{Fe-X} are in agreement with the recent work [24]. To determine the stability of the Fe@C_6N_6 with adsorbed atoms/molecules systems, we calculate the adsorption energy which is expressed as

$$E_{ads} = (E_{Fe-C_6N_6} + E_x) - E_T, \tag{5}$$

where E_T, $E_{Fe-C_6N_6}$ and E_x denotes the total energy of Fe@C_6N_6 with adsorbates, the energy of Fe@C_6N_6 system, and the total energy of an isolated atom or molecules respectively. Positive adsorption energy is an indication of a stable structure. The adsorption energies are listed in Table 3. The calculated results guarantee the chemical adsorption of all the systems.

As can be seen in Table 3, the adsorption of atoms on Fe@C_6N_6 sheet modulates the total magnetic moment per unit cell. The total magnetic moment in Fe@C_6N_6 with adsorbed O and H atoms systems increased whereas we find drastic magnetic moment reduction in Fe@C_6N_6 with adsorbed N and C. The modulation is related to the electron transfer between the Fe

and the surrounding atoms. As illustrated in Table 3, total magnetic moment is high in cases with large charge transfer from Fe into the surrounding atoms as well as the adsorbed atoms (H and O atoms). This shows that interaction between Fe and O, H relatively preserves the number of unpaired electrons in the d orbital of Fe. Thus, the atomic magnetic moment of Fe is maintained in those systems. In contrast, Fe@C_6N_6 with adsorbed N or C atoms produce low spin configurations. TDOS of Fe@C_6N_6 with adsorbed atoms are depicted in Fig. 5. The TDOS figures for Fe@C_6N_6 with adsorbed H and O show semiconductor electronic character whereas Fe@C_6N_6 with adsorbed C and N maintain half-metallic character. The modulation of half-metallic character in Fe@C_6N_6 into semiconductor when adsorbed by H and O is caused by the shift in impurity state towards higher energy.

Next we relaxed the structures of Fe@C_6N_6 with six adsorbed molecules (CH_4, N_2, O_2, H_2, CO, CO_2). The stable adsorption height $h_{\text{Fe-}X}$, the corresponding adsorption energies and the bond lengths $d_{\text{avg}-X}$ of an isolated as well as adsorbed molecules are listed in Table 3. It can be seen that the adsorption heights vary slightly for different molecules. The smaller value of $h_{\text{Fe}-X}$ for adsorbed CO, O_2 and H_2 is an indication of favourable chemical bonding compared to other adsorbed molecules. Correspondingly, their $d_{\text{avg}-X}$ increases after chemisorption. Interestingly, the adsorption energies for CO and O_2 are almost the same. Our results are in disagreement with the recent report [24]. It was reported that O_2 would favourably chemisorbed on the Fe@C_6N_6 surface as compared to CO when the two gases are passed into the surface at constant pressure. We used DFT method in our ground state computations, whereas the work in Ref. [24] employed DFT+U in the similar adsorption environment (different graphitic CN allotrope). Despite such a difference in computational methodology, we do not expect a large discrepancy in the computed adsorption energy. As it turns out, our result is in the same order as that of Ref. [24] since the $h_{\text{Fe}-X}$ for CO and O_2 are almost the same. It indicates strong interaction between CO, O_2 molecules and Fe atom due to hybridization. The computed adsorption energy for CO_2 is within the value suggested by Deng *et al.* [35].

As illustrated in Table 3, high magnetic moment per unit cell are obtained for different Fe@C_6N_6 with adsorbed molecules systems. As can be seen under M_{atom}, the contributions of the magnetic moment in the systems mainly originates from Fe atom. This shows that the high spin configuration of 3d electrons of the Fe atom are maintained. Except for CO and N_2 which couple antiferromagnetically with the Fe atoms, the rest of the molecules

aligned in the same order with the Fe atom. Hence, the increase or decrease in the number of unpaired electrons in the 3d orbitals of the Fe atom determines the total magnetic moment. Figs. 6 show the geometries and TDOS of $Fe@C_6N_6$ with adsorbed molecules. It is seen that the half-metallic character of $Fe@C_6N_6$ system can be tuned into a semiconducting one via adsorption of H_2, O_2 and CH_4 molecules onto its surface.

5. Conclusion

In summary, we have investigated the mechanical, geometrical, electronic and magnetic properties of $Fe@C_6N_6$ system under the influence of external environment based on first-principles calculations. Our findings reveal that the binding energy of $Fe@C_6N_6$ can be modulated by an applied tensile strain and perpendicular electric field. The non-magnetic semiconducting property of bare C_6N_6 is modulated upon embedding of Fe atom in the porous site of the sheet. It is found that the $Fe@C_6N_6$ system exhibits half-metallic electronic character with magnetic moment which is in the order of that for an isolated Fe atom. Additionally, the electronic and magnetic properties of the $Fe@C_6N_6$ systems are preserved under a maximum value of 10 V/nm in electric field strength and 6% tensile strain.

Interestingly, we find that the half-metallic electronic character of $Fe@C_6N_6$ system can be tuned into a semiconductor via adsorption of atoms and molecules into the $Fe@C_6N_6$ system. The appearance of semiconducting character is a result of shift in impurity state towards higher energy when the atoms or molecules are adsorbed on $Fe@C_6N_6$ surface. The magnetic moment of $Fe@C_6N_6$ with adsorbed atoms/molecules is also modified. Our findings may serve as a guide for future applications of $Fe@C_6N_6$ structures in spintronics devices.

Acknowledgments

T. L. Yoon wishes to acknowledge the support of Universiti Sains Malaysia RU grant (No. 1001/PFIZIK/811240). Figures showing atomic model and 2D charge-density difference plots are generated using the XCRYSDEN program Ref. [36]. We gladfully acknowledge Dr. Chan Huah Yong from USM School of Computer Science, and Prof. Mohd. Zubir Mat Jafri from USM School of Physics, for providing us computing resources to carry out part of the calculations done in this paper.

References

[1] Y. Z. Abdullahi, T. L. Yoon, M. M. Halim, M. R. Hashim, M. Z. M. Jafri, L. T. Leng, Geometric and electric properties of graphitic carbon nitride sheet with embedded single manganese atom under bi-axial tensile strain, Current Applied Physics 16 (8) (2016) 809–815.

[2] S. Zhang, R. Chi, C. Li, Y. Jia, Structural, electronic and magnetic properties of 3d transition metals embedded graphene-like carbon nitride sheet: A DFT + U study, Physics Letters A 380 (14) (2016) 1373–1377.

[3] D. Ghosh, G. Periyasamy, B. Pandey, S. K. Pati, Computational studies on magnetism and the optical properties of transition metal embedded graphitic carbon nitride sheets, Journal of Materials Chemistry C 2 (37) (2014) 7943–7951.

[4] A. AlZahrani, Theoretical investigation of manganese adsorption on graphene and graphane: A first-principles comparative study, Physica B: Condensed Matter 407 (6) (2012) 992–1002.

[5] Y. Z. Abdullahi, M. M. Rahman, S. Abubakar, R. Muhida, H. Setiyanto, Low coverage palladium adsorption on graphene: First principles study, Quantum Matter 4 (2015) 430–435.

[6] F. Ersan, O. Arslanalp, G. Gokoglu, E. Akturk, Effect of adatoms and molecules on the physical properties of platinum-doped and-substituted silicene: A first-principles investigation, Applied Surface Science 371 (2016) 314–321.

[7] M. M. Rahman, Y. Z. Abdullahi, A. Shuaibu, S. Abubakar, H. Zainuddin, R. Muhida, H. Setiyanto, Density functional study of structural stabilities, electric and magnetic properties of vanadium adsorption on graphene, Journal of Computational and Theoretical Nanoscience 12 (2015) 1995–2002.

[8] Z. Zhang, Z. Geng, D. Cai, T. Pan, Y. Chen, L. Dong, T. Zhou, Structure, electronic and magnetic properties of hexagonal boron nitride sheets doped by 5d transition metal atoms: First-principles calculations and molecular orbital analysis, Physica E: Low-dimensional Systems and Nanostructures 65 (2015) 24–29.

[9] Y. Yagi, T. M. Briere, M. H. Sluiter, V. Kumar, A. A. Farajian, Y. Kawazoe, Stable geometries and magnetic properties of single-walled carbon nanotubes doped with 3 d transition metals: A first-principles study, Physical Review B 69 (7) (2004) 075414.

[10] E. Kroke, M. Schwarz, E. Horath-Bordon, P. Kroll, B. Noll, A. D. Norman, Tri-s-triazine derivatives. Part I. From trichloro-tri-s-triazine to graphitic C3N4 structures, New Journal of Chemistry 26 (5) (2002) 508–512.

[11] M. Asadpour, S. Malakpour, M. Faghihnasiri, B. Taghipour, Mechanical properties of two-dimensional graphyne sheet, analogous system of BN sheet and graphyne-like BN sheet, Solid State Communications 212 (2015) 46–52.

[12] A. Wang, X. Zhang, M. Zhao, Topological insulator states in a honeycomb lattice of s-triazines, Nanoscale 6 (19) (2014) 11157–11162.

[13] Y. Z. Abdullahi, T. L. Yoon, M. M. Halim, M. R. Hashim, T. L. Lim, Mechanical and electronic properties of graphitic carbon nitride sheet: First-principles calculations, Solid State Communications 248 (2016) 144–150.

[14] Q. H. Wang, K. Kalantar-Zadeh, A. Kis, J. N. Coleman, M. S. Strano, Electronics and optoelectronics of two-dimensional transition metal dichalcogenides, Nature Nanotechnology 7 (11) (2012) 699–712.

[15] X.-H. Li, X. Wang, M. Antonietti, Mesoporous g-C3N4 nanorods as multifunctional supports of ultrafine metal nanoparticles: hydrogen generation from water and reduction of nitrophenol with tandem catalysis in one step, Chem. Sci. 3 (2012) 2170–2174.

[16] J. Zhang, M. Grzelczak, Y. Hou, K. Maeda, K. Domen, X. Fu, M. Antonietti, X. Wang, Photocatalytic oxidation of water by polymeric carbon nitride nanohybrids made of sustainable elements, Chemical Science 3 (2) (2012) 443–446.

[17] X. Zhang, X. Xie, H. Wang, J. Zhang, B. Pan, Y. Xie, Enhanced photoresponsive ultrathin graphitic-phase C3N4 nanosheets for bioimaging, Journal of the American Chemical Society 135 (1) (2012) 18–21.

[18] X. Zhang, H. Wang, H. Wang, Q. Zhang, J. Xie, Y. Tian, J. Wang, Y. Xie, Single layered graphitic-C3N4 quantum dots for twophoton fluorescence imaging of cellular nucleus, Advanced Materials 26 (26) (2014) 4438–4443.

[19] A. Du, S. Sanvito, S. C. Smith, First-principles prediction of metal-free magnetism and intrinsic half-metallicity in graphitic carbon nitride, Physical Review Letters 108 (19) (2012) 197207.

[20] I. Choudhuri, P. Garg, B. Pathak, Tm@gt-C3N3 monolayers: high-temperature ferromagnetism and high anisotropy, Journal of Materials Chemistry C 4 (35) (2016) 8253–8262.

[21] S. Sun, G. Zhang, N. Gauquelin, N. Chen, J. Zhou, S. Yang, W. Chen, X. Meng, D. Geng, M. N. Banis, R. Li, S. Ye, S. Knights, G. A. Botton, T.-K. Sham, X. Sun, Single-atom catalysis using Pt/graphene achieved through atomic layer deposition, Scientific Reports 3 (2013) 1775 EP –, article.

[22] Y. Ji, H. Dong, H. Lin, L. Zhang, T. Hou, Y. Li, Heptazine-based graphitic carbon nitride as an effective hydrogen purification membrane, RSC Advances 6 (57) (2016) 52377–52383.

[23] Z. Ma, X. Zhao, Q. Tang, Z. Zhou, Computational prediction of experimentally possible g-C3N3 monolayer as hydrogen purification membrane, International Journal of Hydrogen Energy 39 (10) (2014) 5037–5042.

[24] D. Ma, Q. Wang, X. Yan, X. Zhang, C. He, D. Zhou, Y. Tang, Z. Lu, Z. Yang, 3d transition metal embedded C2N monolayers as promising single-atom catalysts: A first-principles study, Carbon 105 (2016) 463 – 473.

[25] J. Sirijaraensre, J. Limtrakul, Hydrogenation of CO_2 to formic acid over a Cu-embedded graphene: A DFT study, Applied Surface Science 364 (2016) 241–248.

[26] P. Giannozzi, S. Baroni, N. Bonini, M. Calandra, R. Car, C. Cavazzoni, D. Ceresoli, G. L. Chiarotti, M. Cococcioni, I. Dabo, QUANTUM ESPRESSO: a modular and open-source software project for quantum

simulations of materials, Journal of Physics: Condensed Matter 21 (39) (2009) 395502.

[27] P. Hohenberg, W. Kohn, Inhomogeneous electron gas, Physical Review 136 (3B) (1964) B864.

[28] J. P. Perdew, K. Burke, M. Ernzerhof, Generalized gradient approximation made simple, Physical Review Letters 77 (18) (1996) 3865.

[29] D. Vanderbilt, Soft self-consistent pseudopotentials in a generalized eigenvalue formalism, Physical Review B 41 (11) (1990) 7892.

[30] N. Marzari, D. Vanderbilt, A. De Vita, M. Payne, Thermal contraction and disordering of the Al (110) surface, Physical Review Letters 82 (16) (1999) 3296.

[31] H. J. Monkhorst, J. D. Pack, Special points for Brillouin-zone integrations, Physical Review B 13 (12) (1976) 5188.

[32] E. Cadelano, P. L. Palla, S. Giordano, L. Colombo, Elastic properties of hydrogenated graphene, Physical Review B 82 (23) (2010) 235414.

[33] K. Srinivasu, B. Modak, S. K. Ghosh, Improving the photocatalytic activity of s-triazine based graphitic carbon nitride through metal decoration: an ab initio investigation, Physical Chemistry Chemical Physics 18 (38) (2016) 26466–26474.

[34] P.-O. Lowdin, On the nonorthogonality problem connected with the use of atomic wave functions in the theory of molecules and crystals, The Journal of Chemical Physics 18 (3) (1950) 365–375.

[35] Q. Deng, L. Zhao, X. Gao, M. Zhang, Y. Luo, Y. Zhao, Single layer of polymeric cobalt phthalocyanine: Promising low-cost and high-activity nanocatalysts for CO Oxidation, Small 9 (20) (2013) 3506–3513.

[36] A. Kokalj, Computer graphics and graphical user interfaces as tools in simulations of matter at the atomic scale, Computational Materials Science 28 (2) (2003) 155–168.

Table 1: Calculated lattice parameters and total strain energy for Fe atom embedded striazine system.

Strain (%)	Area (Å^2)	Total energy Biaxial (Ry)	Total energy Uniaxial (Ry)	Lattice parameter Biaxial (Å)
-0.02	167.61	-998.95042	-998.98795	13.91/24.10
-0.015	169.32	-998.97718	-998.99904	13.98/24.22
-0.01	171.05	-998.99598	-999.00600	14.05/24.34
-0.005	172.78	-999.00762	-999.00946	14.13/24.47
0	174.52	-999.01171	-999.01171	14.20/24.59
0.005	176.27	-999.00880	-999.01108	14.27/24.71
0.01	178.03	-998.99980	-999.00779	14.34/24.83
0.015	179.79	-998.98403	-999.00136	14.41/24.96
0.02	181.57	-998.96248	-998.99209	14.48/25.08

Table 2: The calculated binding energies E_b, the average bond length between Fe atom and N_{edge} atoms d_{Fe-N}, average bond length connecting the s-triazine d, and Fe height h (refers to the difference in the z-coordinate of the Fe atom and the average of the z-coordinate of all the C and N atoms in the C_6N_6 sheet). Charge transfer, magnetic moment per unit cell and per Fe atom,electronic character of the Fe@C_6N_6 system are denoted by Q, M_{cell}, M_{Fe}, EC respectively. All the systems are half-metallic.

Strain	E_b (eV)	d_{Fe-N} (Å)	d (Å)	h (Å)	Q (electrons)	M_{Fe} (μ_B)	M_{cell} (μ_B)	EC
0%	4.73	2.06 – 3.40	1.49	-0.01	0.53	3.61	3.74	HM
1%	4.56	2.06 – 3.49	1.51	-0.01	0.54	3.61	3.73	HM
2%	4.05	2.09 – 3.56	1.53	0.00	0.56	3.61	3.71	HM
3%	3.21	2.09 – 3.64	1.55	0.00	0.56	3.61	3.70	HM
4%	2.06	2.02 – 3.80	1.58	0.00	0.53	3.57	3.69	HM
5%	0.75	2.08 – 3.82	1.61	0.00	0.54	3.57	3.66	HM
6%	-0.82	2.08 – 3.91	1.63	0.00	0.56	3.57	3.64	HM

Table 3: E_{ads} denotes calculated adsorption energy. $h_{\text{Fe}-X}$ denotes averaged height between Fe atom and the adsorbates. $d_{\text{avg}-X}$ denotes bond length of molecules. X represents adsorbate species. The values without parenthesis are that for absorbed molecules while that in parenthesis are for isolated molecules. Q refers to net charge transfer among the adsorbates and the Fe@C_6N_6 system. The values without parenthesis are charge transfer from Fe atom into the sheet or adsorbates. These values are all positive as electron from Fe atom always get transferred into the surrounding. The Q values in parenthesis are charge transfer into the Fe-striazine sheet from adsorbates. Positive values mean electron is transferred into the surroundings (Fe@C_6N_6 system) from adsorbates, and vice versa. M_{cell} refers to magnetic moment per unit cell. M_{atom} refers to magnetic moment of Fe atom or adsorbates. The values without parenthesis are that for Fe atom, while that in parenthesis are that for the adsorbates. EC refers to the electronic character of the Fe@C_6N_6 with adsorbates. In the present case, EC can be either half metallic (HM) or semiconducting (SC).

System	E_{ads} (eV)	$h_{\text{Fe}-X}$ (Å)	$d_{\text{avg}-X}$ (Å)	Q (electrons)	M_{cell} (μ_B)	M_{atom} (μ_B)	EC
C	4.48	1.56	-	0.13 (0.19)	1.68	2.17 (-0.71)	HM
N	3.00	1.52	-	0.24 (0.02)	1.56	1.53 (-0.12)	HM
O	4.11	1.65	-	0.54 (-0.34)	4.57	3.45 (0.78)	SC
H	1.90	1.60	-	0.46 (-0.12)	4.31	3.93 (0.11)	SC
CO	1.30	1.89	1.14 (1.16)	0.29 (C: 0.33, O: 0.09)	3.53	3.48 (-0.13)	SC
CO_2	0.44	2.16	1.18 (1.18)	0.50 (C: 0.79, O: -0.41)	3.78	3.64 (0.24)	HM
O_2	1.32	1.82	1.23 (1.40)	0.52 (-0.23)	3.70	3.12 (0.49)	HM
N_2	0.15	2.12	1.11 (1.14)	0.36 (0.2)	3.55	3.51 (-0.15)	HM
H_2	0.31	1.87	0.75 (0.79)	0.42 (0.21)	3.68	3.53 (0.00)	SC
CH_4	0.18	2.16	1.10 (1.10)	0.51 (C: -0.64, H: 0.90)	3.76	3.62 (0.02)	SC

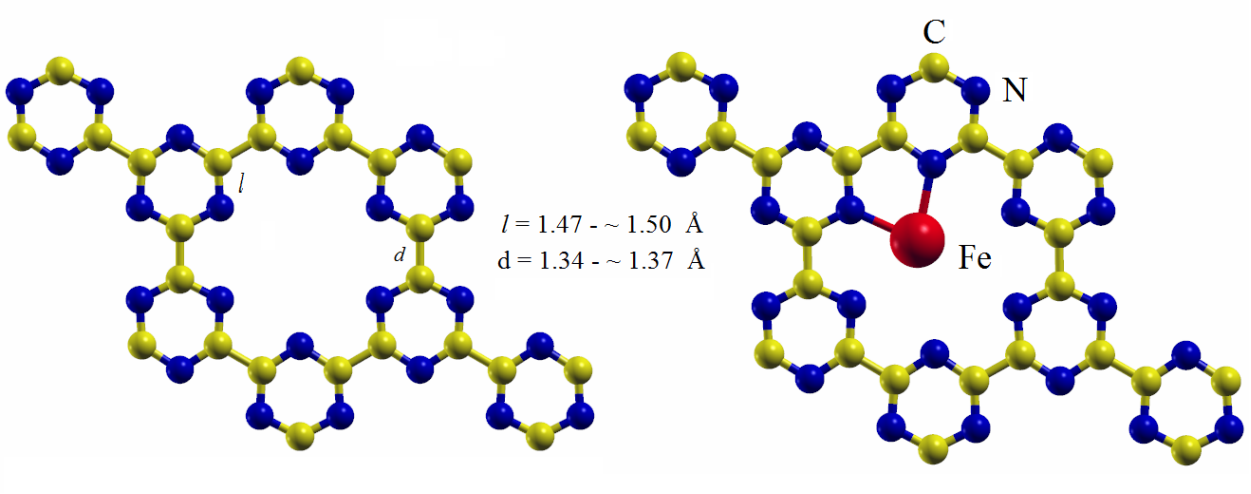

(a)

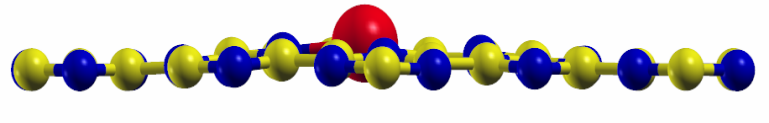

(b)

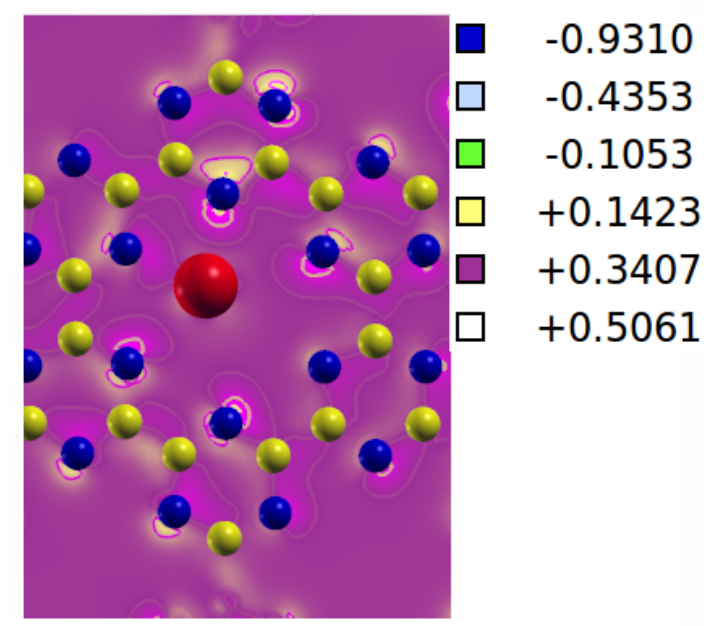

(c)

Figure 1: (a). Relaxed structure of 2×2 C_6N_6 sheet (left panel) and relaxed structure (right) of Fe embedded 2×2 C_6N_6. (b). Relaxed side view of 2×2 C_6N_6 sheet with an embedded Fe atom (Fe@C_6N_6) under perpendicular electric field strength of 10 V/nm. (c). Difference charge-density for Fe atom embedded s-triazine. The color scale shows ranges of charge accumulation and depletion in a.u.

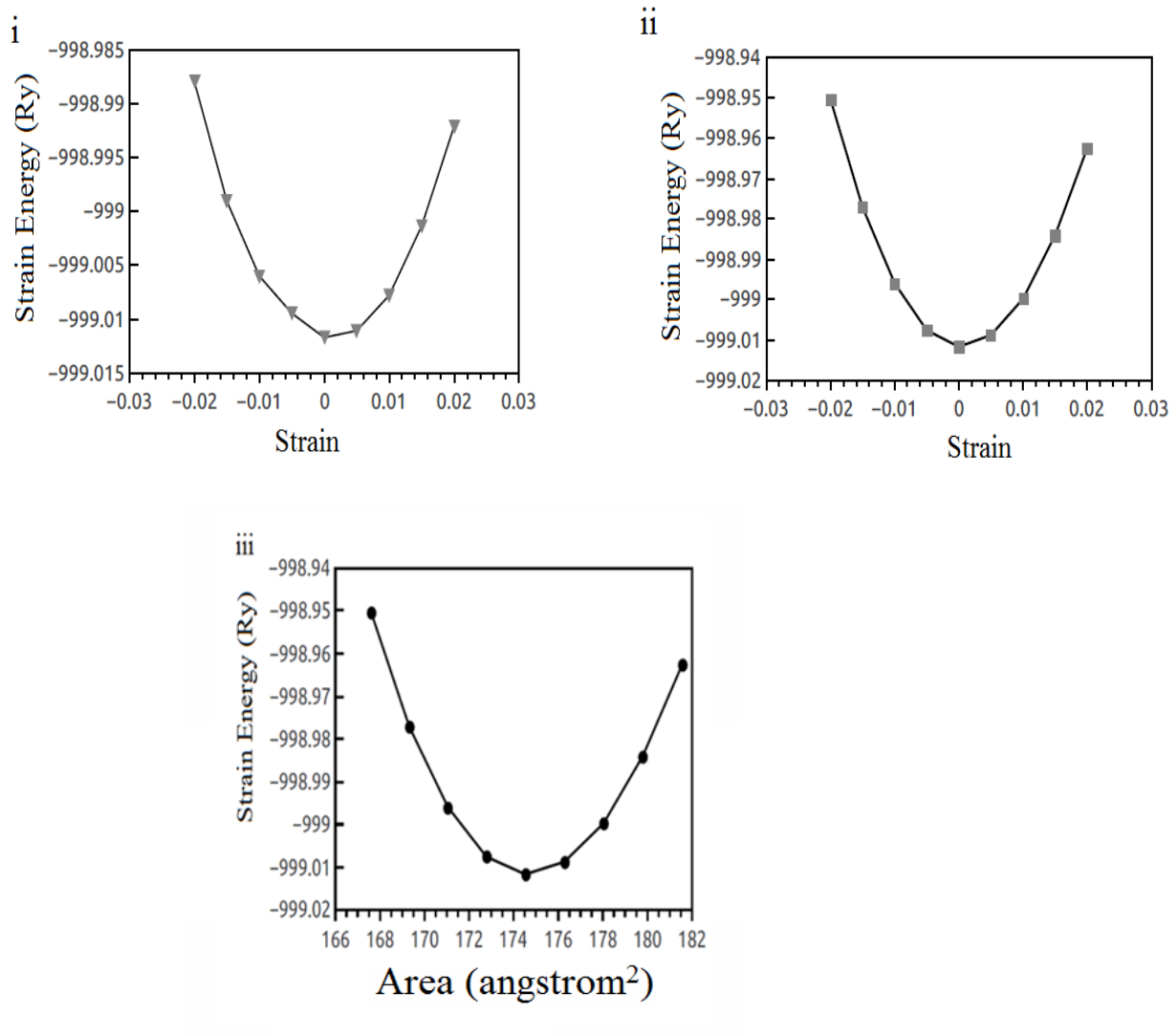

Figure 2: Variation of strain energy (Ry) versus (i) bi-axial tensile strain (ii) uni-axial tensile strain and (iii) area of the Fe@C_6N_6 system for elastic constant calculation.

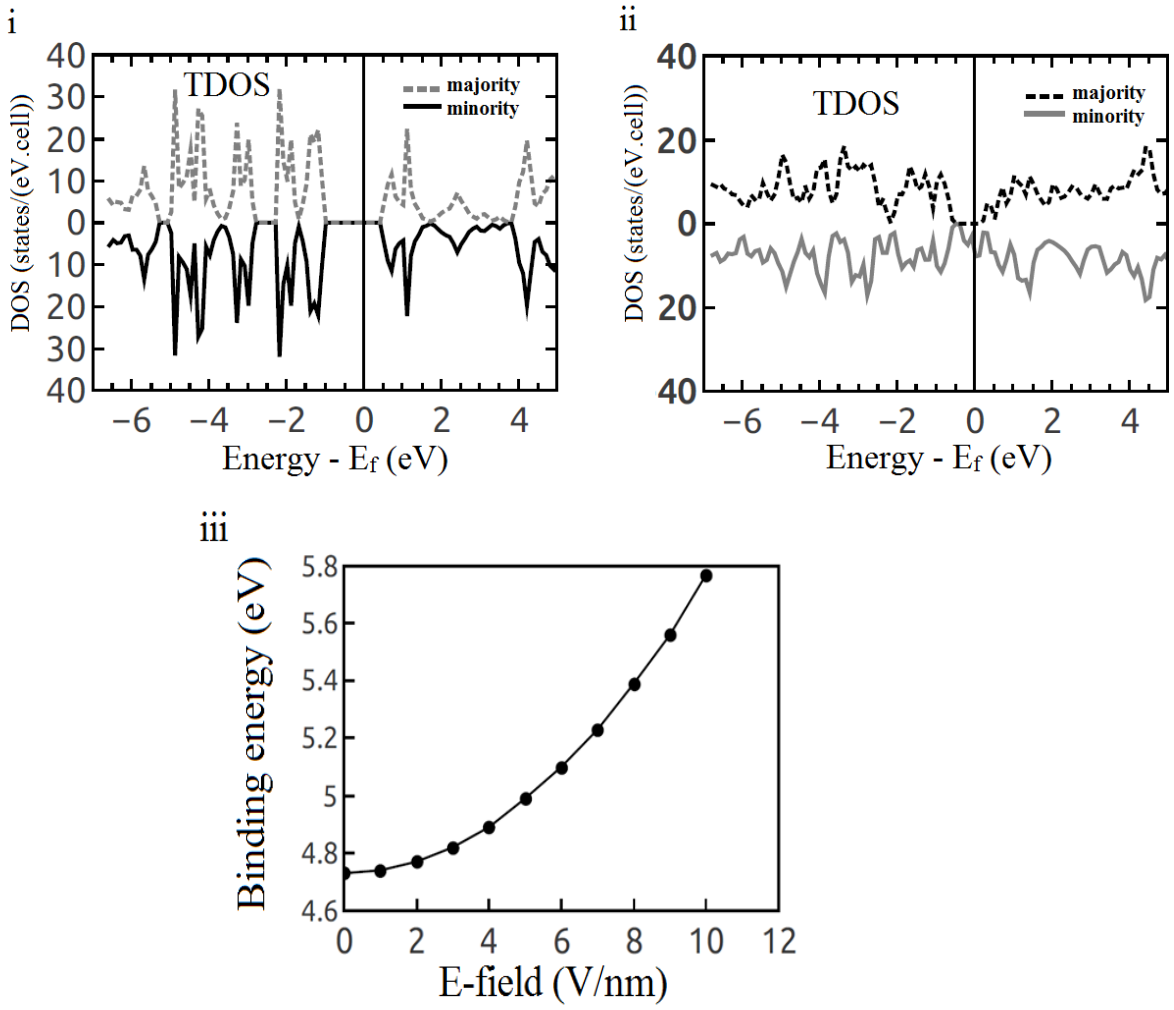

Figure 3: Spin-polarized total density of state (TDOS) for (i) pure s-triazine sheet (ii) $Fe@C_6N_6$ under applied electric field. (ii) Variation of binding energy versus applied electric field strength for $Fe@C_6N_6$ system.

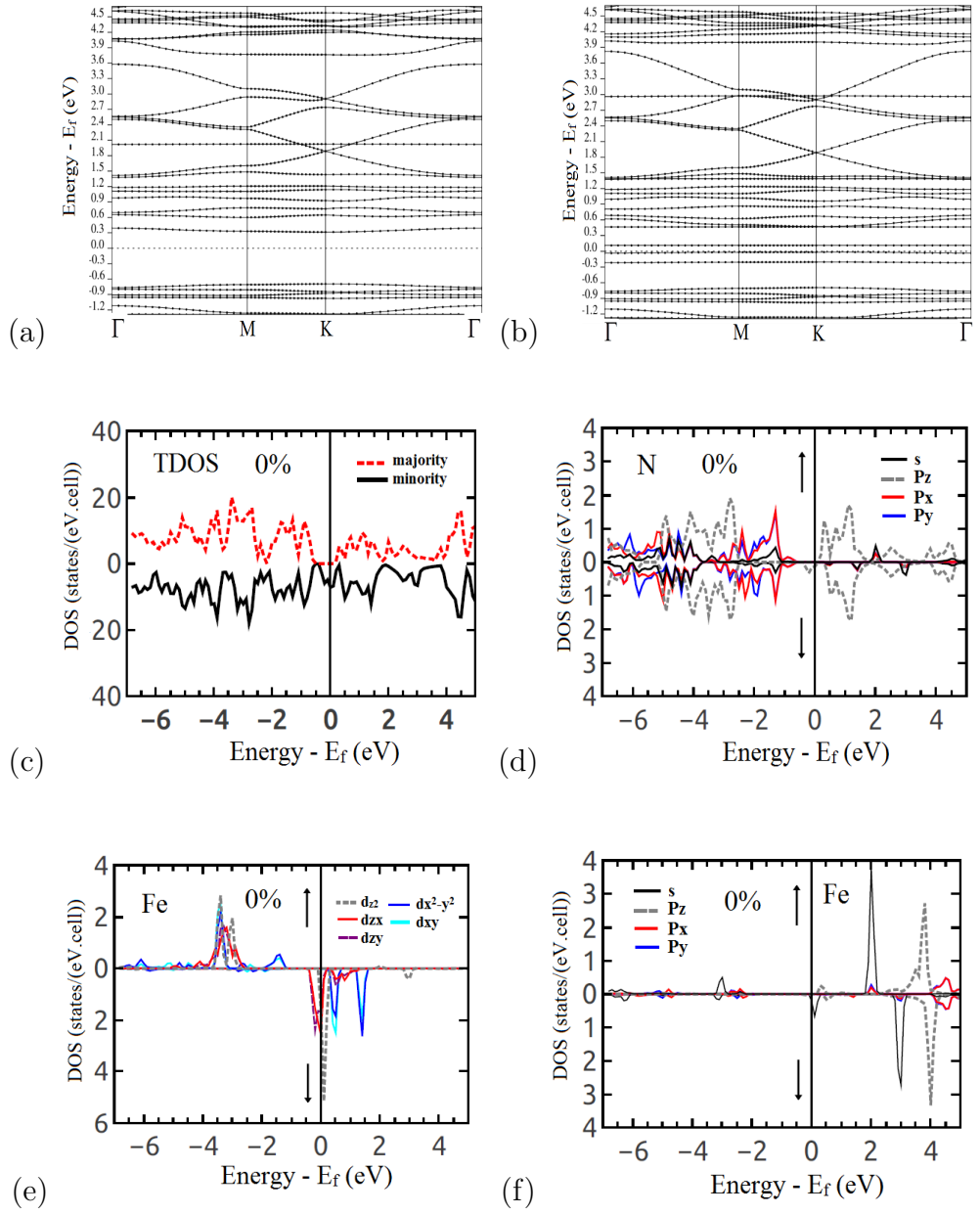

Figure 4: Spin-polarized electronic band structure (a) majority (b) minority spin states for unstrained ($s = 0$) Fe@C_6N_6 system. Spin-polarized TDOS and projected density of state (PDOS) for strain-free (c)-(f).

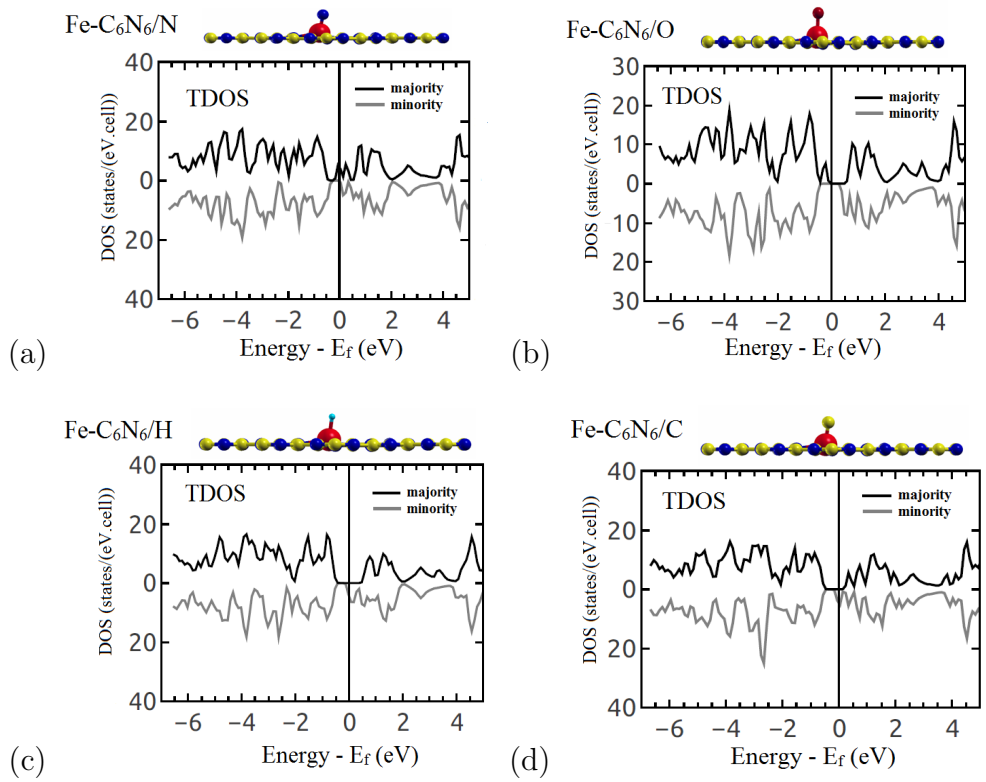

Figure 5: Spin-polarized TDOS and side view for Fe@C_6N_6 with an adsorbed (a) C (b) N (c) O and (d) H atoms systems respectively.

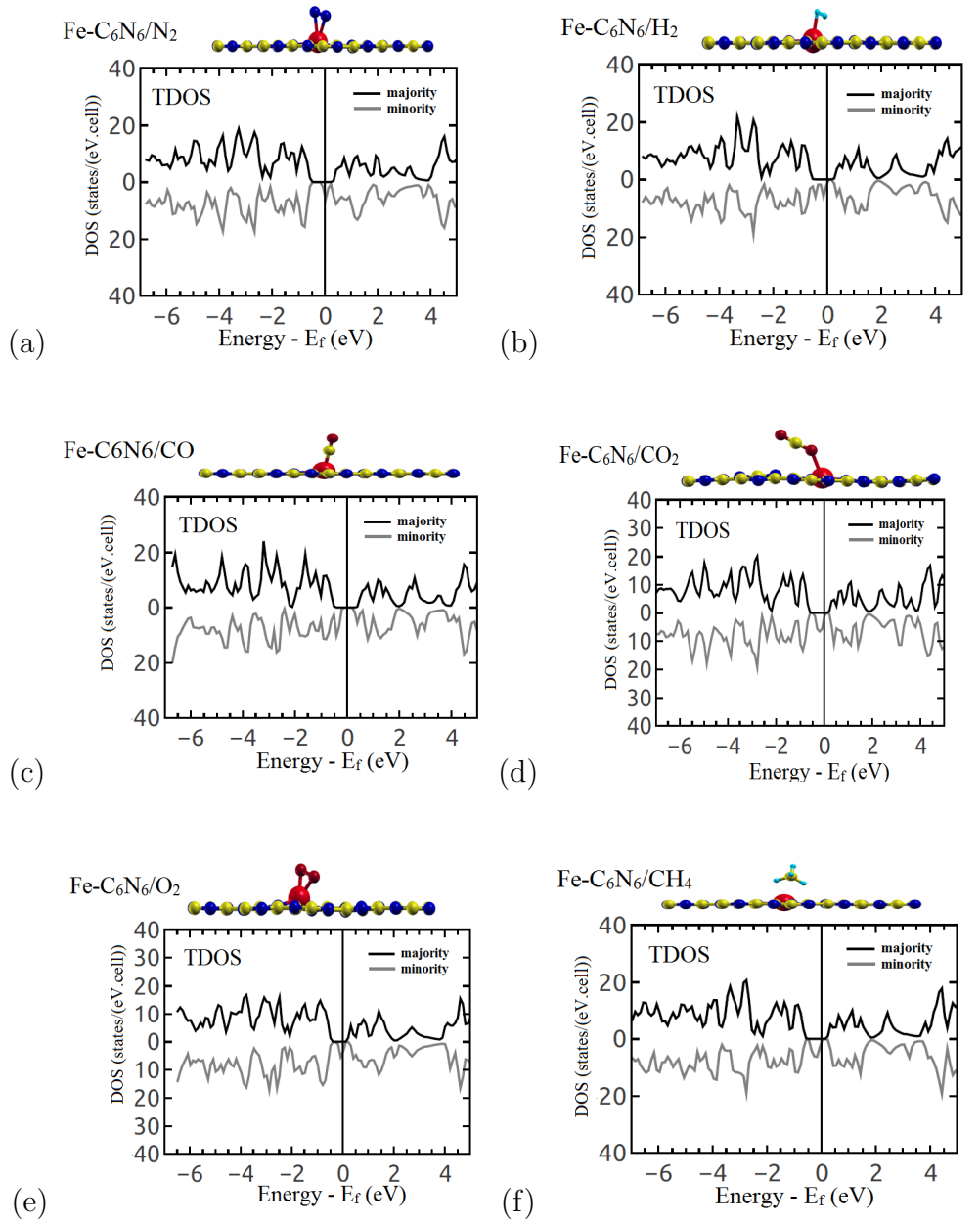

Figure 6: Spin-polarized TDOS and side view for $Fe@C_6N_6$ with an adsorbed (a) N_2 (b) H_2 (c) CO (d) CO_2 (e) O_2 and (f) CH_4 molecules systems respectively.